THE *IRAS* BRIGHT GALAXY SAMPLE. III. 1–10 μm OBSERVATIONS AND COADDED *IRAS* DATA FOR GALAXIES WITH $L_{IR} \geqslant 10^{11}\ L_{\odot}$

DAVID P. CARICO, D. B. SANDERS, B. T. SOIFER, J. H. ELIAS, K. MATTHEWS, AND G. NEUGEBAUER
Palomar Observatory, California Institute of Technology, Pasadena, California 91125
Received 25 August 1987; revised 27 October 1987

ABSTRACT

Galaxies from the *IRAS* Bright Galaxy Sample with infrared luminosities $L_{IR} \geqslant 10^{11}\ L_{\odot}$ have been measured at 1.3, 1.6, 2.2, 3.7, and 10 μm. In addition, coadded *IRAS* measurements at all four *IRAS* bands have been obtained. It is found that an increase in the total infrared luminosity above $L_{IR} \geqslant 10^{11}\ L_{\odot}$ is correlated with increased emission from hot dust with characteristic temperatures $\sim$800 K contributing a substantial fraction of the 2.2 and 3.7 μm emission. This hot dust emission appears to "turn on" at luminosities of roughly $10^{11}\ L_{\odot}$. The far-infrared emission cannot be modeled with a single dust temperature, but requires a cold ($T \sim 30$–50 K) component coupled with a warmer ($T \gtrsim 70$ K) component. Although the relative contribution from the cold component decreases with increasing luminosity, the temperature of the warmer component is independent of luminosity. The $f_{\nu}(12\ \mu m)/f_{\nu}(25\ \mu m)$ ratios for the galaxies in this sample are small compared with other extragalactic objects, indicating that the radiation at 12 and 25 μm is dominated by emission from large dust grains radiating at high temperatures, rather than PAHs. The spatial distribution of the 10 μm emission indicates a substantial extended component for most of the galaxies in this sample, implying that star-formation processes contribute significantly to the luminosities. However, one-third of the galaxies have exponential scale sizes characteristic of compact sources, and half of the galaxies have 10 μm emission consistent with a contribution of 50% or more from a central point source.

I. INTRODUCTION

The *IRAS* Bright Galaxy Sample (Soifer *et al.* 1987, hereafter referred to as Paper I) has helped demonstrate the importance of infrared emission in the energy budget of the local universe. The space density of *IRAS* galaxies is comparable to or greater than that of starburst or Seyfert galaxies, and, at the highest infrared luminosities, *IRAS* galaxies appear to be the most numerous objects known (Paper I). Understanding the nature of this infrared emission is clearly of great importance.

Various analyses have concluded that the excess infrared emission in the vast majority of low to moderately high infrared luminosity galaxies ($L_{IR} \lesssim 10^{11}\ L_{\odot}^{*}$; L_{IR} is defined in Sec. III) is due to star-formation processes, rather than active nuclei (see, for example, Eales *et al.* 1988; Carico *et al.* 1986; Elston, Cornell, and Lebofsky 1985; Rieke *et al.* 1980). However, at the highest luminosities ($L_{IR} \gtrsim 10^{12}\ L_{\odot}$), evidence suggests that active nuclei may be important in infrared galaxies (Becklin and Wynn-Williams 1987; Hill, Wynn-Williams, and Becklin 1987; Sanders *et al.* 1988), and that such galaxies may represent a phase in the formation of quasars (Sanders *et al.* 1988). These results suggest that the luminosity range $10^{11} L_{\odot} < L_{IR} \lesssim 10^{12}\ L_{\odot}$ is a transition range wherein the emergence of active nuclei occurs.

The current paper is one in a series of papers analyzing the properties of the Bright Galaxy Sample. The results of 1–10 μm observations, as well as coadded *IRAS* data, of 61 galaxies from the Bright Galaxy Sample are presented. All of the 61 galaxies have $L_{IR} \geqslant 10^{11}\ L_{\odot}$; thus, they are representative of the most extreme luminosities known. By comparing the galaxies in the current sample with galaxies of both lower luminosity ($L_{IR} < 10^{11}\ L_{\odot}$) and the highest luminosities ($L_{IR} \gtrsim 10^{12}\ L_{\odot}$), it is the intent of this work to investigate the nature of the transition from normal galaxy properties to the extreme properties reported for galaxies with $L_{IR} \geqslant 10^{12}\ L_{\odot}$, and in particular to determine whether the unusual properties of galaxies with $L_{IR} \geqslant 10^{12}\ L_{\odot}$ are found, to a lesser degree, in infrared galaxies at lower luminosities.

II. THE SAMPLE

The galaxies analyzed in this paper are a subset of the *IRAS* Bright Galaxy Sample (Paper I), which contains 324 galaxies, and represents all extragalactic objects with *IRAS* 60 μm flux densities greater than 5.4 Jy in an area of $\sim$14 500 sq. deg, with Galactic latitude $|b| > 30°$, and declination $\delta > -30°$ for 0–12 hr, $\delta > -15°$ for 12–14 hr, and $\delta > -20°$ for 14–24 hr (Paper I).

The selection of galaxies for inclusion in this analysis was based on the far-infrared luminosity L_{FIR}, which is tabulated in Paper I for the Bright Galaxy Sample, and which utilizes the *IRAS* 60 and 100 μm data to obtain an estimate of the luminosity between 40 and 400 μm (see Appendix B of *Cataloged Galaxies and Quasars Observed in the IRAS Survey* (1985)). In order to focus on the most luminous infrared galaxies, a list was compiled of all galaxies from the Bright Galaxy Sample with $L_{FIR} \geqslant 10^{11}\ L_{\odot}$. These galaxies, of which there are 69, will hereafter be referred to as the luminous bright galaxies, or LBGs; they are tabulated in Table I, along with their coordinates and redshifts, reprinted from Paper I, and their optical diameters as measured from the Palomar Observatory Sky Survey prints. Of these 69 galaxies, eight were not observable at the time the Palomar observations were being done. The remaining 61 galaxies, analyzed in this paper, therefore represent an unbiased and nearly complete sample of luminous infrared galaxies.

* Throughout the text, H_0 is taken as 75 km s^{-1} Mpc^{-1}; $L_{\odot}$ is the solar bolometric luminosity, 3.83×10^{26} W.

 0004-6256/88/020356-18$00.90

TABLE I. Identification of galaxies.

NAME	OTHER	RA		–1950–	DEC		REDSHIFT[a]	D_o^b
	NAME	(h)	(m)	(s)	(deg)	(arc m)	(arc s)	(z)	(arc s)
NGC 34	Mrk 938	0	8	33.4	–12	23	10	0.0198	35
MCG–02-01-051	Arp 256	0	16	18.0	–10	39	14	0.0250	35
NGC 232†		0	40	17.5	–23	50	2	0.0208	40
IC 1623	VV114	1	5	18.0	–17	46	37	0.0185	40
MCG–03-04-014		1	7	42.0	–17	7	1	0.0335	25
MCG+02-04-025		1	17	22.8	+14	5	53	0.0311	25
IRAS 0136-10†		1	36	24.0	–10	42	25	0.0475	15
III ZW 035†		1	41	48.0	+16	51	7	0.0274	20
NGC 695	UGC 1315	1	48	28.1	+22	20	10	0.0326	35
NGC 958		2	28	11.8	– 3	9	32	0.0192	100
UGC 2238		2	43	33.4	+12	53	10	0.0208	35
IRAS 0243+213		2	43	49.2	+21	22	44	0.0227	20
UGC 2369		2	51	15.6	+14	46	1	0.0312	40
NGC 1143/4	UGC 2388	2	52	38.6	– 0	23	6	0.0285	65
IRAS 0335+15		3	35	57.1	+15	23	6	0.0353	20
UGC 2982		4	9	43.2	+ 5	25	12	0.0177	35
MCG–03-12-002		4	19	6.5	–18	55	48	0.0316	20
NGC 1614	Mrk 617	4	31	35.8	– 8	40	55	0.0158	50
IRAS 0518-25		5	18	58.6	–25	24	40	0.0424	10
NGC 2623	Arp 243	8	35	25.2	+25	55	48	0.0185	35
IRAS 0857+39		8	57	13.0	+39	15	40	0.0583	20
UGC 4881	Arp 55	9	12	39.6	+44	32	20	0.0399	35
UGC 5101		9	32	4.6	+61	34	37	0.0400	30
MGC+08-18-012†		9	33	18.5	+48	41	53	0.0260	30
IC 563/4†		9	43	44.2	+ 3	17	26	0.0203	
NGC 3110		10	1	32.2	– 6	14	2	0.0161	60
IRAS 1017+08		10	17	22.1	+ 8	28	41	0.0480	10
IRAS 1056+24		10	56	35.5	+24	48	43	0.0417	25
A1101+41	V32	11	1	5.8	+41	7	8	0.0345	35
MCG+00-29-023		11	18	38.6	– 2	42	36	0.0241	20
UGC 6436	IC 2810	11	23	9.8	+14	56	53	0.0341	15
NGC 3690	Mrk 171	11	25	42.0	+58	50	17	0.0105	80
IRAS 1211+03		12	11	12.2	+ 3	5	20	0.0723	15
IRAS 1222-06		12	22	29.0	– 6	24	14	0.0250	15
NGC 4418	UGC 7545	12	24	22.1	– 0	36	14	0.0068	60
MCG+08-23-097		12	48	21.4	+48	12	18	0.0294	25
Mrk 231	UGC 8058	12	54	4.8	+57	8	38	0.0421	30
NGC 4922	UGC 8135	12	59	1.0	+29	34	59	0.0245	45
MCG+01-33-036†		12	59	17.8	+ 4	36	4	0.0362	30
IC 860		13	12	40.1	+24	52	52	0.0129	35
UGC 8335	VII Zw 506	13	13	41.3	+62	23	17	0.0312	30
UGC 8387†	Arp 193	13	18	19.0	+34	23	49	0.0229	60
NGC 5104	UGC 8391	13	18	49.2	+ 0	36	14	0.0186	50
NGC 5256	UGC 8632	13	36	14.2	+48	31	52	0.0276	25
NGC 5257/8	UGC 8641	13	37	22.1	+ 1	5	13	0.0227	115
Mrk 273	UGC 8696	13	42	51.6	+56	8	13	0.0380	70
UGC 8739		13	47	1.7	+35	30	14	0.0171	110
NGC 5331†	VV 253	13	49	41.3	+ 2	21	7	0.0332	40
ZW 247.020	Mrk 1490	14	17	53.8	+49	27	54	0.0260	20
IRAS 1434-14		14	34	52.3	–14	47	24	0.0811	15

TABLE I. (continued)

NAME	OTHER NAME	RA (h)	RA (m)	RA (s)	DEC (deg)	DEC (arc m)	DEC (arc s)	REDSHIFT[a] (z)	D_o^b (arc s)
				–1950–					
UGC 9618	Arp 302	14	54	47.8	+24	48	58	0.0337	80
ZW 049.057		15	10	45.6	+ 7	24	43	0.0118	40
I ZW 107	Mrk 848	15	16	19.0	+42	55	41	0.0401	40
IRAS 1525+36		15	25	3.1	+36	9	0	0.0534	20
Arp 220	UGC 9913	15	32	46.3	+23	40	8	0.0182	50
IRAS 1533-05		15	33	32.4	– 5	13	59	0.0260	40
NGC 6090	UGC 10267	16	10	24.0	+52	35	6	0.0291	25
MCG+01-42-088		16	28	27.4	+ 4	11	24	0.0236	40
NGC 6285/6	Arp 293	16	57	44.9	+59	0	40	0.0187	65
IRAS 1713+53		17	13	14.2	+53	13	52	0.0507	20
MCG–03-57-017		22	28	42.7	–19	17	31	0.0242	50
IRAS 2249-18		22	49	9.6	–18	8	20	0.0760	20
NGC 7469	UGC 12332	23	0	44.6	+ 8	36	18	0.0165	50
ZW 453.062		23	2	28.1	+19	16	55	0.0246	40
ZW 475.056		23	13	31.2	+25	16	48	0.0274	30
NGC 7592	Mrk 928	23	15	47.5	– 4	41	20	0.0244	35
NGC 7674	UGC 12608	23	25	24.7	+ 8	30	14	0.0289	45
NGC 7771		23	48	52.1	+19	49	55	0.0145	110
Mrk 331		23	48	52.8	+20	18	22	0.0180	40

[a] Redshifts are reprinted from Paper I, and are taken as either v/c or DH_o/c where v or D is given in Table 1 or Paper I.

[b] D_o is the optical diameter, as estimated from the Palomar Observatory Sky Survey prints.

III. OBSERVATIONS AND DATA REDUCTION

The 1–10 μm measurements were made at the Cassegrain $f/70$ focus of the Hale 5 m telescope at Palomar Observatory, using a solid-nitrogen-cooled InSb detector system for the 1.3–3.7 μm measurements, and a helium-cooled germanium bolometer for the 10 μm measurements. Beam sizes ranged from 4.6″ to 10″ in diameter, and sky subtraction was achieved by chopping to reference positions 15″ north and south of the galaxy. Sixty-one galaxies were observed at 1.27 μm (J), 1.65 μm (H), and 2.23 μm (K); 58 were observed at 3.69 μm (L'); and 59 were observed at 10.6 μm (N). The bandwidths of the filters used are $\Delta\lambda = 0.24\,\mu$m, $\Delta\lambda = 0.30$ μm, $\Delta\lambda = 0.41$ μm, $\Delta\lambda = 0.64$ μm, and $\Delta\lambda = 4.7$ μm, respectively. The measurements between 1.27 and 3.69 μm were calibrated using standard stars from Elias *et al.* (1982); the 10.6 μm measurements were calibrated at 10.1 μm, using standard stars that are effectively on the system of Tokunaga (1984).

In general, observations were made by first locating the position of maximum flux at 2.2 μm in the beam (the instantaneous signal was always large enough to do this), then measuring fluxes at that location at all wavelengths. The photometric uncertainties for the 1.3, 1.6, and 2.2 μm measurements are generally $< 8\%$, and are primarily due to difficulties in accurately centering in the beam the position of maximum emission in the galaxy. Since the near-infrared flux-density ratios (colors) are relatively independent of beam position, the uncertainties in the ratios are considerably less than those in the individual flux densities. For the 3.7 and 10 μm measurements, the photometric uncertainties are typically $\lesssim 15\%$ and 20%, respectively, but range up to 50% for some sources due to the increased background noise at longer infrared wavelengths.

The LBGs have a broad range of energy distributions. Hence, individual corrections for redshift (K corrections) have been made for each galaxy by using the measured flux densities to estimate by interpolation the flux densities at the filter wavelengths for an equivalent galaxy with zero heliocentric velocity. This process systematically overestimates the flux densities at 3.7 μm, so at that wavelength the interpolated flux density was averaged with the measured flux density for each galaxy to obtain the K correction. Also, this process does not provide corrections for the 10 μm data; however, the uncertainties in the 10 μm data are large enough, and the redshifts small enough, that any correction at 10 μm would be inappropriate. Since the Bright Galaxy Sample was defined to have Galactic latitude $|b| > 30°$, where Galactic extinction is generally small, no corrections have been made for extinction within our own galaxy. Furthermore, no correction was made for internal extinction, because a large fraction of the galaxies in this sample are highly disturbed, and corrections would be difficult to estimate.

A large number of the LBGs contain optically obvious multiple nuclei. In such cases, near-infrared measurements were taken on each nucleus. These individual measurements have been used in calculating the near-infrared flux-density ratios; however, when comparing a 10 μm flux density to *IRAS* data (where typical beam sizes were $1.5' \times 4.75'$), an estimate of the total 10 μm emission, obtained by adding the individual flux densities from all measured positions, has

been used. For all of the galaxies there is clearly a problem when attempting to relate the near-infrared ratios to *IRAS* measurements because of the difference in beam sizes. To minimize this problem, an effort was made to use flux-density ratios from only that position within each source whose near-infrared emission was clearly dominant. However, for 11 of the LBGs, no such dominant position was found, so that both sets of near-infrared measurements have been used throughout the paper, and it is assumed that the infrared luminosity is distributed roughly equally between the individual objects.

Many of the LBGs have only limits listed in the *IRAS Point Source Catalog* (1985) for the 12 μm flux density. The original *IRAS* scans over the galaxies were therefore coadded, providing flux-density estimates down to $\sim$0.4 Jy, which is below the sensitivity limit (0.5 Jy) of the *Point Source Catalog*. For completeness, this procedure was applied to all four *IRAS* bands, although the resulting deviations from the data in Paper I at 60 and 100 μm are small.

Although the LBG sample was selected on the basis of the far-infrared luminosity, $L_{\rm FIR}$ (see Sec. II), for all subsequent analyses the luminosity was adjusted for each galaxy using the method of Perault *et al.* (1987) to estimate $L_{\rm IR}$, the luminosity between 8 and 1000 μm, utilizing all four *IRAS* bands. The resulting luminosity, which will be used throughout the rest of this paper, provides a better estimate of the total infrared luminosity and is systematically higher than $L_{\rm FIR}$; the sample mean and dispersion of $L_{\rm IR}/L_{\rm FIR}$ for the LBGs is 1.30 ± 0.14.

The observed near-infrared and *IRAS* flux densities, as well as the near-infrared beam diameters, are tabulated in Table II, and the *K* corrected near-infrared flux densities are given in Table III. Table IV lists the near-infrared and *IRAS* flux-density ratios used in the analysis, as well as the infrared luminosities $L_{\rm IR}$.

IV. DISCUSSION

a) 1.3–3.7 μm Measurements: The Source of the Near-Infrared Emission

Figure 1 shows the dependence of the near-infrared emission on luminosity for infrared galaxies by plotting the logarithms of the flux-density ratios $R(1.3/1.6) \equiv f_\nu(1.27\,\mu\text{m})/f_\nu(1.65\,\mu\text{m})$ and $R(2.2/1.6) \equiv f_\nu(2.23\,\mu\text{m})/f_\nu(1.65\,\mu\text{m})$ versus luminosity for a broad range of luminosities, where $f_\nu(\lambda)$ is the flux density at wavelength λ. Throughout this paper, the notation $R(\lambda_1/\lambda_2)$ will refer to the appropriate flux density ratio. The lower-luminosity data ($L_{\rm IR} < 10^{11}\ L_\odot$) are from Carico *et al.* (1986), and represent a sample of *IRAS* galaxies (the *IRAS* Minisurvey Sample; see Soifer *et al.* 1984) that was flux-density limited at 0.5 Jy and 60 μm, a factor of 10 fainter than the limit used to define the LBG sample. The two samples have the same mean redshift (the systematically higher luminosity of the LBGs is offset by the higher flux-density limit as compared to the lower-luminosity sample), and hence the only relevant difference in the selection criteria between the lower-luminosity galaxies and the LBG sample is the luminosity cutoff used to define the latter sample. Since 12 and 25 μm data are not available for the lower-luminosity galaxies, the infrared luminosity $L_{\rm IR}$ for those galaxies has been taken as $L_{\rm IR} = 1.3 \times L_{\rm FIR}$, adopting the mean $L_{\rm IR}/L_{\rm FIR}$ for the LBGs given above; $L_{\rm IR}/L_{\rm FIR}$ is not correlated with $L_{\rm IR}$ for the LBGs. The dashed lines in Fig. 1, at $\log[R(1.3/1.6)] = -0.09$ and $\log[R(2.2/1.6)] = -0.12$, represent the ratios appropriate for normal spiral galaxies (Aaronson 1977).

From Fig. 1 it is clear that the extreme 8–1000 μm luminosities of the LBGs are also reflected in the near-infrared emission. The near-infrared flux-density ratios deviate more from normal galaxy colors with increasing wavelength, as evidenced by the larger change in $R(2.2/1.6)$ compared to $R(1.3/1.6)$ for $L_{\rm IR} \gtrsim 10^{11}\ L_\odot$. Further, Fig. 1(b) suggests that the mechanisms affecting the near-infrared emission "turn on" at luminosities of roughly $10^{11}\ L_\odot$. This indicates a means of selecting highly luminous galaxies based on near-infrared emission alone. By using $R(2.2/1.6) \sim 1$ ($\log[R(2.2/1.6)] \sim 0$ or $[H-K] \sim 0.5$ mag) as a rough cutoff, one should be able, on average, to separate out unusually infrared-luminous galaxies from more normal objects. As this procedure would require only broadband 1.6 and 2.2 μm measurements, it may prove extremely useful, particularly since such infrared-luminous galaxies generally have large amounts of visual extinction, making the optical spectra more difficult to obtain.

The near-infrared flux-density ratios $R(1.3/1.6)$, $R(2.2/1.6)$, and $R(3.7/1.6)$ for the LBGs are shown in Fig. 2. This figure is a three-dimensional representation, where the ratios are plotted on the *x*, *y*, and *z* axes, respectively, of a standard right-handed coordinate system. To eliminate ambiguities in the apparent position of the data in this three-dimensional space, the projection of the data onto each of the axis planes is also shown.

Figure 2 shows that the dispersion in the near-infrared properties of the LBGs is largest at 3.7 μm (note the different scale used for the $R(3.7/1.6)$ axis in Fig. 2). This effect cannot be attributed entirely to the larger statistical uncertainties in the 3.7 μm data; the dispersion in $R(3.7/1.6)$ due to uncertainties in the measurements is roughly twice that in $R(2.2/1.6)$, whereas the observed range in $R(3.7/1.6)$ is almost four times that in $R(2.2/1.6)$. The 3.7 μm data were not included in Fig. 1, since 3.7 μm measurements are not available for the lower-luminosity galaxies. However, Fig. 2 indicates that $R(3.7/1.6)$ is correlated with $R(2.2/1.6)$, indicating that the increase in luminosity beyond $10^{11} L_\odot$ apparently affects the near-infrared flux-density ratios at longer wavelengths. Furthermore, the LBGs with $L_{\rm IR} \geqslant 10^{12}\ L_\odot$ all have $R(3.7/1.6)$ ratios that are among the largest in the sample, indicating a significant luminosity dependence of the $R(3.7/1.6)$ ratio.

Included in Fig. 2 are representative flux-density ratios for normal galaxy emission (N), a "starburst" nucleus (B), and an active galactic nucleus, or AGN (A). $R(3.7/1.6)$ for a normal galaxy is taken to be 0.43 (Lawrence *et al.* 1985). The flux-density ratios used for an AGN are those of the quasar 3C 273 (from Neugebauer *et al.* 1987); throughout this paper the term AGN will refer specifically to a quasar-like energy source. The flux-density ratios used for a starburst nucleus are those of the nucleus of the archetypal starburst galaxy NGC 253. The 1.2–2.2 μm measurements for NGC 253 are from Scoville *et al.* (1985), and the 3.7 μm flux density (taken to be equal to the published 3.5 μm measurement) is from Becklin, Fomalont, and Neugebauer (1973).

Figure 2 presents a direct comparison of the near-infrared continuum emission of the LBGs to that of other extragalactic sources. It is seen that the near-infrared flux-density ratios of most of the LBGs lie roughly between the ratios expected for normal galaxies and those of active nuclei, and are

TABLE II. Observed flux densities.

NAME	OBS CODE[a]	BEAM[b] (arc sec)	$f_\nu(\lambda)$, PALOMAR (mJy)[c] 1.3 μm	1.6 μm	2.2 μm	3.7 μm	10 μm	$f_\nu(\lambda)$, IRAS (Jy)[c] 12 μm	25 μm	60 μm	100 μm
NGC 34		5.0	23.02	35.44	37.17	44.84	251.31	0.36	2.15	17.85	16.6
MCG–02-01-051		5.0	5.94	8.66	8.36	9.03	122.52	0.26	1.43	6.68	10.21
IC 1623†	(a)	5.0	8.06	9.41	7.28	4.44		0.80	4.18	22.65	34.08
	(b)	5.0	8.67	14.50	16.53		158.56				
	(c)	10.0	16.52	24.52	27.18	31.89					
	(d)	10.0	15.78	18.43	15.07	<30.46					
MCG–03-04-014		5.0	11.54	16.96	16.68	13.54	83.21	0.39	1.02	5.49	11.49
MCG+02-04-025†	(a)	5.0	1.53	1.88	1.52	1.66	<31.64	0.32	1.63	10.27	10.78
	(b)	5.0	6.40	8.50	8.59	12.70	113.82				
	(c)						128.29				
NGC 695		5.0	10.62	14.50	13.75	10.66	52.99	0.49	0.97	7.75	14.83
NGC 958		5.0	12.77	17.44	14.94	6.60	<32.23	0.76	1.51	5.55	16.10
UGC 2238		5.0	7.76	14.24	16.38	14.05	89.58	0.39	0.76	8.35	16.69
IRAS 0243+213		10.0	13.00	17.92	16.68	11.69	57.04	0.14	1.19	5.71	7.07
UGC 2369†	(a)	5.0	8.91	12.29	10.82	5.24	<31.35	0.25	1.67	7.86	12.38
	(b)	5.0	5.08	7.47	8.06	9.54	150.04				
NGC 1143/4†	(a)	5.0	8.67	10.70	8.52	3.50	<31.64	0.51	0.69	5.19	12.80
	(b)	5.0	11.64	15.19	14.13	11.58	<34.69				
IRAS 0335+15†	(a)	10.0	4.35	5.77	5.84	7.58	39.83	0.3	0.66	5.80	7.56
	(b)	10.0	2.46	3.17	2.57						
UGC 2982	(a)	5.0	8.13	13.35	13.37	10.37	69.22	0.60	0.80	8.5	18.6
	(b)	10.0	17.46	27.89	28.99						
MCG–03-12-002†	(a)	5.0	6.40	8.19	9.00	5.80	27.30	0.27	0.56	5.52	10.52
	(b)	10.0	11.86	16.35	15.21						
	(c)	5.0	4.55	6.75	7.08	5.44	30.49				
	(d)	10.0	6.83	9.58	9.51						
NGC 1614	(a)	5.0	34.21	48.47	49.00	51.01	832.15	1.57	8.24	30.40	37.67
	(b)	10.0	42.28	59.90	59.46	63.05					
IRAS 0518-25	(a)	5.0	12.89	27.38	52.75	122.37	515.47	0.76	3.52	13.94	11.68
	(b)	10.0	14.39	29.75	55.75	123.50					
NGC 2623		5.0	9.33	15.05	18.12	13.54	160.03	0.34	2.16	23.52	28.66
IRAS 0857+39†	(a)	5.0	0.91	1.44	3.68	39.78	207.11	0.35	1.73	7.53	4.59
	(b)	10.0	1.41	1.97	4.35	40.52					
	(c)	10.0	1.80	2.47	4.77	37.64	<51.55				
	(d)	10.0	1.61	2.38	4.47	43.62	288.54				
UGC 4881		5.0	4.35	6.51	6.58	4.24	28.85	0.17	0.68	5.99	10.65
UGC 5101	(a)	5.0	8.59	13.60	22.82	30.46	136.84	0.25	1.05	12.09	20.07
	(b)	10.0	12.89	20.02	27.43	31.02					
NGC 3110		5.0	11.12	15.76	14.53	11.90	61.97	0.64	1.31	11.32	23.03
IRAS 1017+08†	(a)	10.0	17.62	16.50	10.82			0.26	1.35	5.56	6.29
	(b)	10.0	3.27	4.18	3.86	2.88	10.48				
IRAS 1056+24		10.0	11.12	15.76	16.99	18.35	182.05	0.23	1.44	12.09	17.99
A1101+41		5.0	5.42	7.90	8.36	9.20	80.95	<0.16	0.47	6.67	11.63
MCG+00-29-023		7.0	17.30	24.07	24.79	20.88	122.52	0.34	0.79	5.53	10.03
UGC 6436		5.0	5.57	7.97	7.84	3.87	34.37	0.20	0.81	5.70	11.00
NGC 3690†	(a)	5.0	22.81	32.92	38.21	80.11	895.78	4.75	28.71	112.13	127.82
	(b)	5.0	5.78	8.12	14.66	31.60	273.02				
	(c)	5.0	12.42	20.96	25.25	32.48	483.28				

TABLE II. (continued)

NAME	OBS CODE[a]	BEAM[b] (arc sec)	$f_\nu(\lambda)$, PALOMAR (mJy)[c] 1.3 μm	1.6 μm	2.2 μm	3.7 μm	10 μm	$f_\nu(\lambda)$, IRAS (Jy)[c] 12 μm	25 μm	60 μm	100 μm
IRAS 1211+03		5.0	1.80	2.76	3.24	2.09	53.98	<0.18	0.63	8.36	9.91
IRAS 1222-06		10.0	3.33	4.46	3.62		<26.80	<0.11	1.15	5.46	7.95
NGC 4418		5.0	10.72	14.11	12.31	8.01	398.29	1.1	11.0	43.7	32.0
MCG+08-23-097		5.0	7.48	11.21	11.23	7.04	58.10	<0.11	0.51	4.80	9.11
Mrk 231	(a)	5.0	45.51	100.33	182.91	343.30	1213.95	1.81	8.52	33.60	30.89
	(b)	10.0	48.54	101.26	189.77	379.90					
NGC 4922†	(a)	5.0	4.64	6.88	8.75	21.07	205.21	0.31	1.52	5.39	7.95
	(b)	5.0	16.22	19.84	15.93	7.11	<26.31				
IC 860		5.0	8.13	10.60	9.34	5.24	25.13	0.09	1.31	16.0	19.6
UGC 8335†	(a)	5.0	7.62	11.31	12.31	15.84	201.47	0.41	2.24	11.24	13.78
	(b)	5.0	4.23	6.16	6.23	<6.08	27.81				
NGC 5104		5.0	14.13	21.95	21.99	17.69	90.41	0.22	0.74	6.97	14.25
NGC 5256†	(a)	5.0	7.62	9.94	8.59	6.19	<77.30	0.34	1.15	7.36	11.51
	(b)	5.0	7.55	11.41	11.54	11.16	91.24				
NGC 5257/8†	(a)	5.0	4.64	6.39	5.89	4.48	<69.86	0.58	1.54	10.83	19.63
	(b)	5.0	6.22	8.35	7.15	4.36	<46.58				
	(c)						68.58				
Mrk 273		5.0	8.59	12.99	15.21	16.74	118.09	0.31	2.33	23.70	22.31
UGC 8739		5.0	5.04	9.76	11.33	8.70		0.32	0.46	5.86	16.20
ZW 247.020		5.0	8.44	12.40	12.08	10.27	124.80	0.19	0.99	5.84	9.40
IRAS 1434-14		5.0	1.61	2.41	3.18		<151.43	0.09	0.56	6.82	7.49
UGC 9618		5.0	6.70	12.06	14.26			0.68	0.91	6.22	15.68
ZW 049.057		5.0	6.76	9.58	9.00	5.86	40.95	0.14	0.99	20.50	33.63
I ZW 107		5.0	5.62	7.47	8.06	9.03	104.76	0.25	1.68	9.09	10.84
IRAS 1525+36		5.0	2.92	3.89	3.89	3.70	67.33	0.15	1.32	7.50	5.86
Arp 220	(a)	5.0	9.16	17.44	21.79	21.86	212.91	0.46	8.11	104.08	117.69
	(b)	10.0	18.80	30.58	33.90	24.64					
IRAS 1533-05		5.0	7.55	13.23	14.80	12.93	<183.74	0.15	0.66	5.32	9.42
NGC 6090†	(a)	10.0	13.00	16.65	15.50	11.58	87.94	0.31	1.30	6.22	10.35
	(b)	10.0	5.13	5.77	5.18	4.32	<24.00				
	(c)						23.13				
MCG+01-42-088		5.0	10.92	16.05	16.08	12.35	64.30	0.30	0.91	6.97	13.26
NGC 6285/6		10.0	17.62	28.15	30.08	17.21	34.37	0.37	0.67	8.44	24.80
IRAS 1713+53†	(a)	5.0	5.57	8.19	8.92	10.46	83.99	0.15	0.76	5.92	8.99
	(b)	5.0	2.14	2.76	2.69		<28.07				
MCG-03-57-017		5.0	10.14	15.61	16.68	18.69	124.80	0.31	0.98	5.34	10.28
IRAS 2249-18		5.0	2.02	2.59	2.46	<2.21	<38.74	<0.12	0.57	5.54	4.64
NGC 7469		5.0	52.25	81.18	109.20	156.92	787.41	1.41	5.44	27.2	37.5
ZW 453.062		5.0	5.84	8.66	8.75	6.42	34.37	0.27	0.60	7.31	11.13
ZW 475.056		5.0	12.19	17.60	19.69	18.52	175.47	0.30	2.05	8.92	12.83
NGC 7592†	(a)	5.0	6.34	9.07	8.59	8.39	54.98	0.36	1.15	8.15	11.60
	(b)	5.0	6.11	8.42	8.06	8.08	74.51				
NGC 7674		5.0	9.96	16.50	24.79	59.11	394.64	0.68	2.04	5.22	8.81
NGC 7771		5.0	17.79	27.63	28.20	21.27	114.87	0.83	1.72	19.4	43.0
Mrk 331		5.0	25.95	36.43	34.85	29.09	273.02	0.57	2.52	18.3	22.8

[a] Some of the galaxies were measured with more than one beam diameter, and some at more than one position. For such cases, the Observation Code labels the individual measurements, and can be used to identify these measurements in Tables III and IV. Galaxies measured at more than one position, indicated by †, are discussed in more detail in the notes to Table II.
[b] The diameter of the 1.3–3.7 μm beam; at 10 μm the beam diameter was 4.6″ for all observations. See the *IRAS Explanatory Supplement* (1985) for a discussion of the *IRAS* beam sizes.
[c] The symbol < indicates an upper limit.

Notes to TABLE II
(Offset positions given here are only approximate)

IC 1623. This object contains a number of visible knotlike structures, although it was not possible at the time of the observations to determine which of these structures are separate nuclei. Measurements (a) and (d) are of the visual (also the 2.2 μm) peak, lying in the northwesternmost position of the entire object. Measurements (b) and (c) are of the easternmost position, 15″ east of (a) and (d).
MCG +024-24-025. There are three visually obvious nuclei; the nucleus in measurement (a) is the northernmost nucleus, (b) is 10″ south of (a), and (c) is 5″ east of (b).
UGC 2369. There are two visually obvious nuclei; the nucleus in measurement (a) is 20″ northwest of the nucleus in measurement (b).
NGC 1143/4. There are two visually obvious nuclei; the nucleus in measurement (a) is 40″ west, 20″ north of the nucleus in measurement (b).
IRAS 0335+15. There are two visually obvious nuclei; the nucleus in measurement (a) is 10″ east of the nucleus in measurement (b).
MCG −03-12-002. There are two visually obvious nuclei; the nucleus in measurements (a) and (b) is 20″ north of the nucleus in measurements (c) and (d).
IRAS 0857+39. There are two visually obvious nuclei; measurements (a), (b), and (c) are centered between the two nuclei; measurement (d) is centered on the northwesternmost nucleus.
IRAS 1017+08. There are two visually obvious nuclei; measurement (a) is to the east of measurement (b).
NGC 3690. This object has a distorted morphology with a number of knotlike structures. Measurement (a) is the visual peak; measurements (b) and (c) are east and north of (a), respectively.
NGC 4922. There are two visually obvious nuclei; the nucleus in measurement (a) is 10″ north, 20″ east of the nucleus in measurement (b).
UGC 8335. There are two visually obvious nuclei; the nucleus in measurement (a) is 40″ southeast of the nucleus in measurement (b).
NGC 5256. There are two visually obvious nuclei; measurement (a) is north of measurement (b).
NGC 5257/8. There are two visually obvious nuclei; the nucleus in measurement (a) is northwest of the nucleus in measurement (b); measurement (c) is of a knotlike structure to the southwest of (b).
NGC 6090. There are two visually obvious nuclei; the nucleus in measurement (a) is 10″ northeast of the nucleus in measurement (b); measurement (c) was taken midway between (a) and (b).
IRAS 1713+53. There are two visually obvious nuclei; measurement (a) is northeast of measurement (b).
NGC 7592. There are two visually obvious nuclei; measurement (a) is east of measurement (b).

thus consistent with a combination of normal galaxy emission plus direct emission from an AGN. However, based on their near-infrared ratios, many of the LBGs are also consistent with combinations of normal galaxy emission and emission from a starburst nucleus.

The source of the near-infrared emission in the LBGs is investigated further in Fig. 3, where $R(1.3/1.6)$, $R(2.2/1.6)$, and $R(10/3.7)$ are plotted against $R(3.7/1.6)$. The components A and B from Fig. 2 are indicated in Figs. 3(a) and 3(b). Since the ratios are plotted on a linear scale, with a common wavelength for the denominator, the flux-density ratios for combined contributions from any two components will lie on a straight line connecting the flux-density ratios of the two individual components. Also shown in Figs. 3(a) and 3(b) are trajectories of the following physical processes:

(i) absorption by dust uniformly mixed with the emitting source (line a); the line indicates the reddening produced on the flux-density ratios of a normal galaxy by gradually increasing the optical depth, using the near-infrared reddening law from Cohen *et al.* (1981);

(ii) thermal emission at temperatures of 600 K (line b), 800 K (line c), and 1000 K (line d), with λ^{-1} emissivity, appropriate for dust grains (see, for example, Draine and Lee 1984). The lines emanate from the point corresponding to a normal galaxy, and indicate the change in the flux-density ratios of a normal galaxy as the contribution to the 3.7 μm flux density from thermal emission gradually increases relative to the contribution at 3.7 μm from a normal galaxy. Lines b, c, and d will be taken as representative of contributions from hot dust emission to a normal galaxy component.

From Figs. 3(a) and 3(b), the observed near-infrared ratios of the LBGs are generally consistent with the effects of dust applied to a normal galaxy component. The range in $R(1.3/1.6)$ indicates dust absorption, as seen most clearly in Fig. 3(a). For most of the galaxies, the inferred optical depth at V is between 0 and 10, although for a few objects this number may be much larger. The large dispersion in $R(3.7/1.6)$ cannot be due to extinction (line a), but is consistent with contributions from hot-dust emission with characteristic temperature $\sim$800 K. This contribution is between 0% and 80% of the total 3.7 μm emission for most of the galaxies, while for a few of the objects the data suggest contributions of more than 90%.

If a contribution from direct AGN emission is used to model the flux-density ratios of the LBGs, then contributions ranging from 0% to 50% of the total 3.7 μm emission, in combination with dust absorption and emission, would yield the observed flux-density ratios for most of the LBGs. Hence, there is flexibility in modeling the relative contributions from direct AGN emission and hot-dust emission, and various combinations are allowed by the data. However, given the quantities of dust expected in these objects, as inferred from the far-infrared emission (Paper I), it is likely that most AGN emission would be absorbed and reradiated by the dust, and that the dominant factor contributing to the shift in the near-infrared properties of the LBGs relative to those of a normal galaxy is an increase in hot-dust emission, with characteristic temperature $T\sim$800 K.

In Fig. 3(c), the $R(10/3.7)$ ratio has been plotted as a diagnostic of the relative contribution from hot-dust emission ($T\sim$800 K), responsible for the dispersion in $R(3.7/1.6)$, and warm-dust emission ($T\sim$300–400 K), required to produce significant 10 μm emission. The main result from Fig. 3(c) is that, although there is essentially no correlation between $R(10/3.7)$ and $R(3.7/1.6)$ for most of the LBG sample, it appears that those galaxies with the most extreme $R(3.7/1.6)$ ratios, i.e., those postulated in the previous discussion to contain the most hot dust, all have comparatively low $R(10/3.7)$ ratios. This effect can be explained in two ways, as either due to a shift in the temperature of the dust to hotter temperatures in these galaxies, or an increase in silicate absorption at 10 μm, as the result of a larger mass of dust in these galaxies. These two explanations cannot be distinguished based on the data in this paper.

Identifying the observed near-infrared properties as dominated by dust absorption and emission does not severely con-

TABLE III. Near-infrared flux densities corrected for redshift.

NAME	OBS CODE[a]	$f_\nu(\lambda)$ (mJy)[b] 1.3 μm	1.6 μm	2.2 μm	3.7 μm
NGC 34		24.21	36.26	38.18	49.48
MCG–02-01-051		6.30	8.85	8.60	10.36
IC 1623	(a)	8.29	9.43	7.29	4.44
	(b)	9.14	14.89	16.53	
	(c)	17.28	25.14	27.84	31.89
	(d)	16.24	18.53	15.74	<30.46
MCG–03-04-014		12.48	17.50	17.01	16.09
MCG+02-04-025	(a)	1.62	1.89	1.58	1.98
	(b)	6.81	8.78	9.07	14.99
NGC 695		11.37	14.89	13.97	12.55
NGC 958		13.29	17.59	14.78	7.25
UGC 2238		8.29	14.68	16.62	15.61
IRAS 0243+213		13.65	18.23	16.80	13.07
UGC 2369	(a)	9.53	12.50	10.69	6.15
	(b)	5.47	7.77	8.39	11.38
NGC 1143/4	(a)	9.11	10.76	8.35	4.07
	(b)	12.30	15.51	14.38	13.24
IRAS 0335+15	(a)	4.66	5.99	6.15	9.07
	(b)	2.63	3.20	2.57	
UGC 2982	(a)	8.54	13.59	13.49	11.34
	(b)	18.31	28.45	28.99	
MCG–03-12-002	(a)	6.79	8.54	9.04	6.79
	(b)	12.69	16.74	15.21	
	(c)	4.91	7.00	7.19	6.39
	(d)	7.31	9.88	9.51	
NGC 1614	(a)	35.44	49.26	49.84	63.05
	(b)	43.80	60.83	60.51	55.65
IRAS 0518-25	(a)	15.04	31.37	58.81	151.26
	(b)	16.73	33.95	61.92	152.62
NGC 2623		9.81	15.51	18.27	14.95
IRAS 0857+39	(a)	1.06	1.83	5.05	54.01
	(b)	1.60	2.43	5.87	40.52
	(c)	2.03	2.98	6.32	48.76
	(d)	1.84	2.86	6.06	59.73
UGC 4881		4.79	6.78	6.62	5.23
UGC 5101	(a)	9.54	15.17	24.25	37.23
	(b)	14.27	21.73	28.79	37.90
NGC 3110		11.53	15.94	14.67	12.88
IRAS 1017+08	(a)	18.26	16.14	10.82	
	(b)	3.57	4.33	3.94	3.66
IRAS 1056+24		12.20	16.59	17.81	23.08
A1101+41		5.87	8.22	8.70	11.06
MCG+00-29-023		18.23	24.71	25.19	23.57
UGC 6436		6.02	8.23	7.75	4.65
NGC 3690	(a)	23.37	33.45	39.19	84.65
	(b)	5.92	8.38	15.04	33.34
	(c)	12.80	21.33	25.64	34.38

TABLE III. (continued)

NAME	OBS CODE[a]	$f_\nu(\lambda)$ (mJy)[b] 1.3 μm	1.6 μm	2.2 μm	3.7 μm
IRAS 1211+03		2.15	3.08	3.27	3.31
IRAS 1222-06		3.50	4.49	3.62	
NGC 4418		10.86	14.16	12.32	8.34
MCG+08-23-097		8.04	11.54	11.26	8.22
Mrk 231	(a)	53.33	113.89	200.28	421.43
	(b)	56.41	115.39	208.85	379.90
NGC 4922	(a)	4.92	7.19	9.34	24.00
	(b)	16.91	19.95	15.72	7.99
IC 860		8.34	10.68	9.32	5.58
UGC 8335	(a)	8.21	11.77	12.88	18.82
	(b)	4.55	6.36	6.41	<7.09
NGC 5104		14.82	22.36	22.23	19.38
NGC 5256	(a)	8.04	10.08	8.68	7.20
	(b)	8.08	11.74	11.84	12.90
NGC 5257/8	(a)	4.87	6.49	5.95	5.09
	(b)	6.52	8.43	7.16	4.93
Mrk 273		9.43	13.76	15.90	20.44
UGC 8739		5.33	10.01	11.43	8.70
ZW 247.020		8.97	12.69	12.30	11.84
IRAS 1434-14		1.95	2.81	3.18	
UGC 9618		7.43	12.71	20.77	
ZW 049.057		6.94	9.67	9.02	6.21
I ZW 107		6.09	7.85	8.45	11.29
IRAS 1525+36		3.25	4.09	4.08	5.08
Arp 220	(a)	9.73	18.00	22.19	26.25
	(b)	19.76	31.34	34.14	29.53
IRAS 1533-05		8.16	13.71	15.08	14.94
NGC 6090	(a)	13.73	17.01	15.69	13.48
	(b)	5.34	5.88	5.28	<5.01
MCG+01-42-088		11.54	16.43	16.26	13.89
NGC 6285/6		18.53	28.80	30.04	18.69
IRAS 1713+53	(a)	6.27	8.73	9.51	13.79
	(b)	2.35	2.89	2.69	
MCG–03-57-017		10.78	16.08	17.17	21.15
IRAS 2249-18		2.32	2.75	2.60	<3.53
NGC 7469		54.52	83.92	112.28	170.10
ZW 453.062		6.19	8.88	8.84	7.26
ZW 475.056		12.98	18.27	20.16	21.44
NGC 7592	(a)	6.70	9.25	8.79	9.50
	(b)	6.44	8.60	8.26	9.20
NGC 7674		10.79	17.67	26.75	68.60
NGC 7771		18.46	28.06	28.39	22.83
Mrk 331		27.00	36.98	35.26	31.96

[a] See Table 2.

[b] The symbol < indicates an upper limit.

TABLE IV. Derived quantities.

NAME	OBS CODE[a]	FLUX DENSITY RATIOS[b] R(1.3/1.6)	R(2.2/1.6)	R(3.7/1.6)	R(10/3.7)	R(12/25)	R(25/60)	R(100/60)	$R_{10}^{b,c}$	LOG[$L_{IR}/L_{\odot}$]
NGC 34		0.67	1.05	1.36	5.08	0.17	0.12	0.93	1.01	11.42
MCG–02-01-051		0.71	0.97	1.17	11.83	0.18	0.21	1.53	0.72	11.32
IC 1623	(a)	0.88	0.77	0.47		0.19	0.18	1.50	0.28	11.55
MCG–03-04-014		0.71	0.97	0.92	5.17	0.38	0.19	2.09	0.28	11.54
MCG+02-04-025	(b)	0.78	1.03	1.71	7.59	0.20	0.16	1.05	1.17	11.63
NGC 695		0.76	0.94	0.84	4.22	0.51	0.13	1.91	0.13	11.64
NGC 958		0.76	0.84	0.41	<4.44	0.50	0.27	2.90	<0.04	11.18
UGC 2238		0.56	1.13	1.06	5.74	0.51	0.09	2.00	0.29	11.26
IRAS 0243+213		0.75	0.92	0.72	4.36	0.12	0.21	1.24	0.61	11.14
UGC 2369	(a)	0.76	0.86	0.49	<5.10	0.15	0.21	1.58	0.91	11.58
	(b)	0.70	1.08	1.46	13.18					
NGC 1143/4	(a)	0.85	0.78	0.38	<7.77	0.74	0.13	2.47	<0.15	11.41
	(b)	0.79	0.93	0.85	<2.62					
IRAS 0335+15	(a)	0.78	1.03	1.51	4.39	0.45	0.11	1.30	0.17	11.52
	(b)	0.82	0.80							
UGC 2982	(a)	0.63	0.99	0.83	6.10	0.75	0.09	2.19	0.14	11.15
MCG–03-12-002	(a)	0.80	1.06	0.80	3.20	0.48	0.10	1.91	0.26	11.43
	(c)	0.70	1.03	0.91	4.36					
NGC 1614	(a)	0.72	1.01	1.13	14.95	0.19	0.27	1.24	0.83	11.57
IRAS 0518-25	(a)	0.49	1.82	4.50	3.38	0.22	0.25	0.84	0.92	12.11
NGC 2623		0.63	1.18	0.96	10.70	0.16	0.09	1.22	0.73	11.53
IRAS 0857+39	(d)	0.64	2.12	20.88		0.20	0.23	0.61	20.76	12.08
UGC 4881		0.71	0.98	0.77	5.52	0.25	0.11	1.78	0.23	11.68
UGC 5101	(a)	0.63	1.60	2.45	3.68	0.24	0.09	1.66	0.75	12.01
NGC 3110		0.72	0.92	0.81	4.81	0.49	0.12	2.03	0.12	11.22
IRAS 1017+08	(b)	0.82	0.91	0.85	2.86	0.19	0.24	1.13	0.05	11.82
IRAS 1056+24		0.74	1.07	1.39	7.89	0.16	0.12	1.49	1.18	11.99
A1101+41		0.71	1.06	1.35	7.32	<0.34	0.07	1.74	>0.68	11.58
MCG+00-29-023		0.74	1.02	0.95	5.20	0.43	0.14	1.81	0.46	11.26
UGC 6436		0.73	0.94	0.56	7.39	0.25	0.14	1.93	0.24	11.55
NGC 3690	(a)	0.70	1.17	2.53	10.58	0.17	0.26	1.14	0.54	11.91

1988AJ.....95..356C

TABLE IV. (continued)

NAME	OBS CODE[a]	FLUX DENSITY RATIOS[b] R(1.3/1.6)	R(2.2/1.6)	R(3.7/1.6)	R(10/3.7)	R(12/25)	R(25/60)	R(100/60)	$R_{10}^{b,c}$	LOG[$L_{IR}/L_{\odot}$]
IRAS 1211+03		0.70	1.06	1.07	16.31	<0.29	0.08	1.19	>0.44	12.25
IRAS 1222-06		0.78	0.81			<0.10	0.21	1.46		11.24
NGC 4418		0.77	0.87	0.59	47.76	0.10	0.25	0.73	0.69	11.13
MCG+08-23-097		0.70	0.98	0.71	7.07	<0.22	0.11	1.90	>0.76	11.34
Mrk 231	(a)	0.47	1.76	3.70	2.88	0.21	0.25	0.92	0.89	12.50
NGC 4922	(a)	0.68	1.30	3.34	8.55	0.20	0.28	1.48	0.95	11.31
	(b)	0.85	0.79	0.40	<3.29					
IC 860		0.78	0.87	0.52	4.50	0.07	0.08	1.23	0.45	11.10
UGC 8335	(a)	0.70	1.09	1.60	10.70	0.18	0.20	1.23	0.70	11.76
	(b)	0.72	1.01	<1.11	>3.92					
NGC 5104		0.66	0.99	0.87	4.66	0.30	0.11	2.04	0.55	11.13
NGC 5256	(a)	0.80	0.86	0.71	<10.74	0.30	0.16	1.56	0.36	11.49
	(b)	0.69	1.01	1.10	7.07					
NGC 5257/8	(a)	0.75	0.92	0.78	<13.72	0.38	0.14	1.81	0.16	11.50
	(b)	0.77	0.85	0.58	<9.45					
Mrk 273		0.69	1.16	1.49	5.78	0.13	0.10	0.94	0.57	12.14
UGC 8739		0.53	1.14	0.87		0.70	0.08	2.76		11.07
ZW 247.020		0.71	0.97	0.93	10.54	0.19	0.17	1.61	0.99	11.34
IRAS 1434-14		0.69	1.13			0.16	0.08	1.10		12.27
UGC 9618		0.58	1.63			0.75	0.15	2.52		11.70
ZW 049.057		0.72	0.93	0.64	6.59	0.14	0.05	1.64	0.44	11.07
I ZW 107		0.78	1.08	1.44	9.28	0.15	0.18	1.19	0.64	11.86
IRAS 1525+36		0.79	1.00	1.24	13.25	0.11	0.18	0.78	0.73	12.00
Arp 220	(a)	0.54	1.23	1.34	8.85	0.06	0.08	1.13	0.82	12.19
IRAS 1533-05		0.60	1.10	1.09	<12.30	0.23	0.12	1.77	<1.83	11.27
NGC 6090	(a)	0.81	0.92	0.79		0.24	0.21	1.66	0.51	11.49
	(b)	0.91	0.90	0.85						
MCG+01-42-088		0.70	0.99	0.85	4.63	0.33	0.13	1.90	0.28	11.34
NGC 6285/6		0.64	1.04	0.65	1.84	0.55	0.08	2.94	0.11	11.30
IRAS 1713+53	(a)	0.72	1.09	1.58	6.09	0.20	0.13	1.52	0.79	11.87
	(b)	0.81	0.93							
MCG–03-57-017		0.67	1.07	1.32	5.90	0.32	0.18	1.93	0.54	11.23

TABLE IV. (continued)

NAME	OBS CODE[a]	FLUX DENSITY RATIOS[b] R(1.3/1.6)	R(2.2/1.6)	R(3.7/1.6)	R(10/3.7)	R(12/25)	R(25/60)	R(100/60)	$R_{10}^{b,c}$	LOG[$L_{IR}/L_{\odot}$]
IRAS 2249-18		0.84	0.95	<1.28	~10.98	<0.21	0.10	0.84	~0.47	12.12
NGC 7469		0.65	1.34	2.03	4.63	0.26	0.20	1.38	0.76	11.58
ZW 453.062		0.70	1.00	0.82	4.73	0.45	0.08	1.52	0.16	11.31
ZW 475.056		0.71	1.10	1.17	8.18	0.15	0.23	1.44	0.89	11.54
NGC 7592	(a)	0.72	0.95	1.03	5.79	0.31	0.14	1.42	0.49	11.36
	(b)	0.75	0.96	1.07	8.10					
NGC 7674		0.61	1.51	3.88	5.75	0.33	0.39	1.69	0.77	11.50
NGC 7771		0.66	1.01	0.81	5.03	0.48	0.09	2.22	0.17	11.34
Mrk 331		0.73	0.95	0.86	8.54	0.23	0.14	1.25	0.70	11.43

[a] See Table 2.

[b] $R(\lambda_1/\lambda_2) \equiv f_\nu(\lambda_1)/f_\nu(\lambda_2)$. The symbols < and > indicate that the ratios are upper and lower limits, respectively, where a lower limit in the ratio is due to an upper limit in the flux density in the denominator of the ratio; the symbol ~ indicates that both flux densities (numerator and denominator) in the ratio are upper limits.

[c] R_{10} represents the degree of concentration of the 10 μm emission about the nucleus (see text).

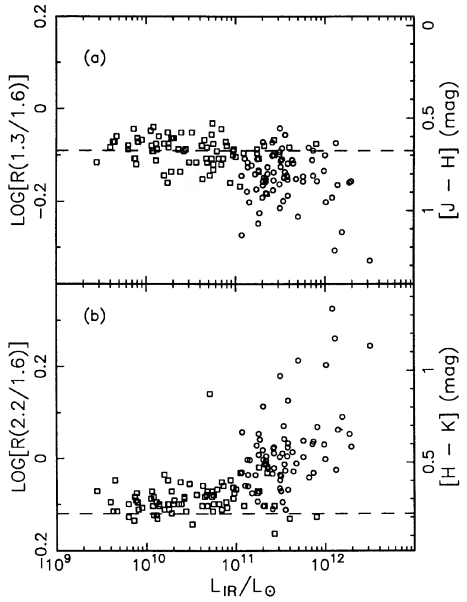

FIG. 1. The near-infrared flux-density ratios (a) $R(1.3/1.6)$ and (b) $R(2.2/1.6)$, plotted logarithmically, versus the infrared luminosity, for the LBGs (circles) and a sample of *IRAS* galaxies studied by Carico *et al.* (1986; squares). L_{IR} is an estimate of the luminosity between 8 and 1000 μm (see the text). The dashed lines indicate representative ratios for normal galaxies (from Aaronson 1977).

strain the intrinsic source of the luminosity in the LBGs. Regions of recent or ongoing star formation would be characterized by large quantities of dust, affecting the near-infrared properties through absorption, as well as emission from hot dust in the environments of very young stars. As was seen in Fig. 2, the flux-density ratios for many of the LBGs are consistent with a contribution from a starburst nucleus. However, for a heavily dust-enshrouded AGN, one would also expect the near-infrared emission to be dominated by dust emission. This is seen in the fact that the LBGs with $L_{IR} \geqslant 10^{12}\ L_{\odot}$, which Sanders *et al.* (1988) have identified as probably containing active nuclei, have near-infrared flux-density ratios that can be readily modeled as due to hot-dust emission. Hence, the near-infrared ratios cannot be used to narrow down the luminosity range wherein the transition to a dominant active nucleus occurs.

There is one galaxy from the LBG sample, IRAS 0857 + 39, which is clearly distinct, due to its extremely large $R(3.7/1.6)$ ratio of 26.56. This galaxy, with a luminosity of $1.2\times10^{12}\ L_{\odot}$, has been studied by Sanders *et al.* (1988), who claim that its primary source of power is an AGN. Such an extreme 3.7 μm excess, although unique in comparison to all of the other LBGs, and certainly inconsistent with direct AGN emission, can be modeled by invoking a substantial emission component from dust at $\sim$500 K.

b) IRAS Data

The luminosity dependence of the far-infrared emission is shown in Fig. 4, where logarithms of the *IRAS* flux-density ratios $R(100/60)$, $R(25/60)$, and $R(12/25)$ are plotted versus L_{IR}. Figure 4(a) is essentially the high-luminosity end of Fig. 6(a) in Paper I, which shows $f_{\nu}(60\ \mu m)/f_{\nu}(100\ \mu m)$ plotted against L_{FIR} for the entire Bright Galaxy Sample. As mentioned previously (Sec. III), the 60 and 100 μm *IRAS* data included in this paper do not differ significantly from those given in Paper I.

The effects seen in Fig. 4(a), namely an apparent minimum $R(100/60)$ ratio, which is independent of luminosity, and an apparent maximum $R(100/60)$, which decreases with increasing luminosity, have been attributed to an effective maximum in the radiation field heating the radiating material, which is independent of luminosity, and an effective minimum in the radiation field which increases with luminosity (Paper I). A similar effect has been found for Seyfert galaxies; see, for example, Miley, Neugebauer, and Soifer (1985).

In Fig. 4(b), there does not appear to be any change in $R(25/60)$ with luminosity above $10^{11}\ L_{\odot}$. This lack of correlation between $R(25/60)$ and infrared luminosity for infrared galaxies does, in fact, continue down to luminosities $\sim10^{9}\ L_{\odot}$, as demonstrated by Smith *et al.* (1987) using another flux-limited sample of *IRAS* galaxies.

In Fig. 4(c), the $R(12/25)$ ratio changes with luminosity in the sense that although almost half of the galaxies in the luminosity range $1\text{–}5\times10^{11}\ L_{\odot}$ have $\log[R(12/25)] > -0.5$ [$R(12/25) > 0.3$], none of the galaxies with $L_{IR} > 5\times10^{11}\ L_{\odot}$ have $\log[R(12/25)] > -0.5$. Thus, there appears to be an absence of galaxies with very high luminosities and high $R(12/25)$ ratios.

The far-infrared flux-density ratios for the LBGs can be compared to those of other extragalactic objects in Fig. 5, where characteristic flux-density ratios for normal (N), starburst (B), and Seyfert (S) galaxies are included. The points N, B, and S were determined based on the data from Rowan-Robinson and Crawford (1986), and are consistent with data from other authors (see, for example, Sekiguchi 1987; Helou 1986; Miley, Neugebauer, and Soifer 1985). Since all of the LBGs are visually extended sources, Seyfert galaxies were chosen to represent the far-infrared flux-density ratios of active galaxies, rather than the quasar 3C 273; any far-infrared disk emission detected by the large-beam *IRAS* measurements is thus taken into account in the comparison.

The far-infrared flux-density ratios for most of the LBGs are similar to those of normal and starburst galaxies. They are distinct from Seyfert galaxies in the $R(25/60)$ ratio, which is typically larger in Seyfert galaxies, reflecting their relatively flat energy distributions. In particular, it is worth emphasizing that the LBGs with $L_{IR} \geqslant 10^{12}\ L_{\odot}$, which appear to be powered by active nuclei (Sanders *et al.* 1988), do not have far-infrared emission consistent with typical Seyfert galaxies. One striking feature of Fig. 5 is that, for a number of the LBGs, the $R(12/25)$ ratios are considerably smaller than the characteristic ratios for normal, starburst, or Seyfert galaxies indicating unusually steep energy distributions between 12 and 25 μm.

To investigate the source of the far-infrared emission in the LBGs, Fig. 5(b) shows the locus of points corresponding to the flux-density ratios for steady-state emission from dust grains, with λ^{-1} emissivity, at a range of temperatures. It can be readily seen that the far-infrared emission in most of the LBGs cannot be modeled with a single dust temperature, but requires at least two components. The data suggest a cold-dust component, with characteristic temperatures

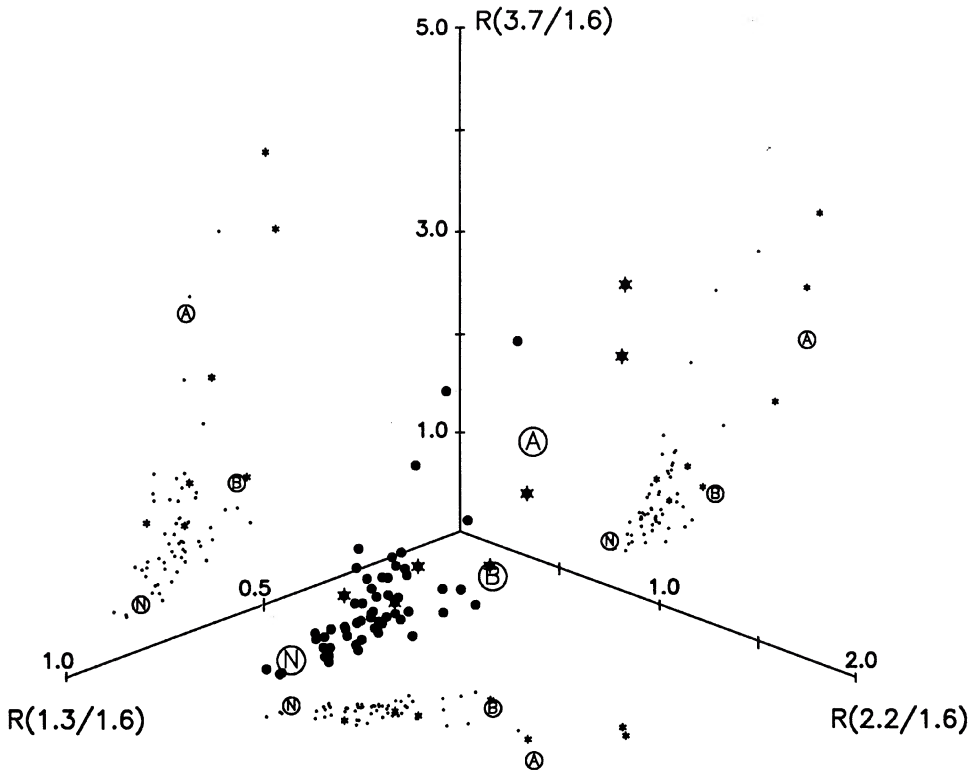

FIG. 2. Near-infrared flux-density ratios $R(1.3/1.6)$, $R(2.2/1.6)$, and $R(3.7/1.6)$. The LBGs previously studied by Sanders *et al.* (1988) are plotted with an asterisk. The data are plotted on the x, y, and z axes of a standard right-handed coordinate system. The smaller circles and asterisks indicate the projections of the data onto each of the axis planes. Note that, due to the different dispersions in the ratios, different scales have been used for the different axes. Also shown are the flux-density ratios representative of normal galaxies (N), active galactic nuclei (A), and starburst nuclei (B). For point N, $R(1.3/1.6)$ and $R(2.2/1.6)$ are from Aaronson (1977), and $R(3.7/1.6)$ is from Lawrence *et al.* (1985). Point A is from Neugebauer *et al.* (1987). For point B, $R(1.3/1.6)$ and $R(2.2/1.6)$ are from Scoville *et al.* (1985), and $R(3.7/1.6)$ is from Becklin, Fomalont, and Neugebauer (1973).

$T \sim 30$–50 K, for most of the galaxies, coupled with a contribution from an additional warmer component, at temperatures $T \gtrsim 70$ K. Such temperatures are in agreement with the results of Sekiguchi (1987) for his sample of starburst galaxies, but are higher than those expected for lower-luminosity *IRAS* galaxies (see, for example, Paper I; De Jong *et al.* 1984) and reflect the decrease in $R(100/60)$ with luminosity seen in Paper I. The highest temperature consistent with the data is probably appropriate for the cold-dust component, since the mass of dust required to produce a given luminosity scales roughly with temperature as T^{-5}.

As Fig. 5(b) shows, the relative contribution to the far-infrared emission from cold ($T \sim 30$–50 K) dust is primarily reflected in the $R(100/60)$ ratio. Thus, the luminosity dependence seen in Fig. 4(a) indicates that, although galaxies with little or no contribution from cold dust are found over the entire luminosity range, as L_{IR} increases, fewer and fewer galaxies are found that have significant quantities of cold dust contributing to their infrared luminosity. This is essentially equivalent to the result from Paper I mentioned previously. The lack of any correlation between $R(25/60)$ and luminosity seen in Fig. 4(b) suggests that the characteristic temperature of the dust with $T \gtrsim 70$ K does not change systematically with luminosity.

Figure 6, which shows log $[R(12/25)]$ vs log $[R(100/60)]$, presents the interesting result that $R(12/25)$ and $R(100/60)$ are correlated. Thus, as $R(12/25)$ increases, indicating a higher characteristic temperature for the dust emitting at 12 and 25 μm, the increase in $R(100/60)$ indicates a colder temperature for the dust emitting at 60 and 100 μm. A plausible explanation for this correlation has been proposed by Helou (1986). Various authors (see, for example, Desert 1986; Puget, Leger, and Boulanger 1985; Sellgren 1984) have discussed the possibility that very small grains ($\sim$ a few Angstroms in size), transiently heated to roughly 1000 K, can be an important source of emission at wavelengths between 1 and 20 μm. Evidence suggests that these small grains are polycyclic aromatic hydrocarbons, known as PAHs (Leger and Puget 1984). In Helou's model, the $R(12/25)$ ratio reflects the relative contributions from PAHs and from larger, hot-dust grains radiating in a steady state. For relatively quiescent, inactive galaxies, $R(12/25)$ is affected by the emission from PAHs in the 12 μm band, resulting in large $R(12/25)$ ratios. As the intensity of the

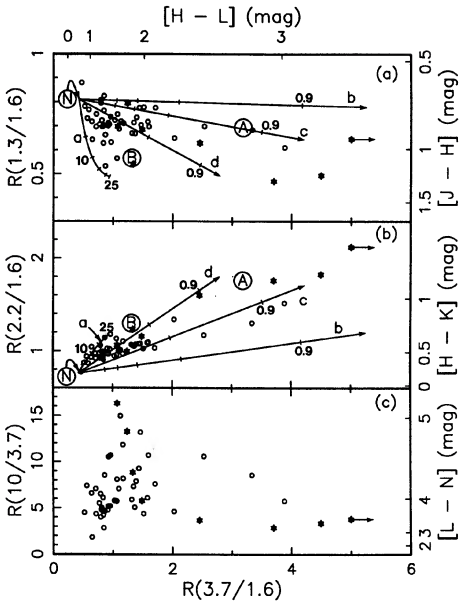

FIG. 3. Flux-density ratios $R(1.3/1.6)$, $R(2.2/1.6)$, and $R(10/3.7)$, plotted against $R(3.7/1.6)$. The LBGs previously studied by Sanders *et al.* (1988) are plotted with an asterisk. Galaxies with only limits at 3.7 or 10 μm have been excluded. The lines a through d represent the following: a = absorption from dust uniformly mixed with the source, labeled as a function of the optical depth at V, τ_v, where $I_v \propto \tau_v^{-1}(1 - e^{-\tau_v})$; b, c, and d = contributions from hot-dust emission at $T = 600$, 800, and 1000 K, respectively; the tick marks indicate the fraction of the total 3.7 μm emission from dust emission, relative to normal-galaxy emission, and are drawn at intervals of 10%. The arrows point toward the flux-density ratios of pure hot-dust emission (no contribution from a normal galaxy). The lines a through d extend from the point representative of normal galaxies (from Aaronson (1977) and Lawrence (1985); see the text). Also shown are the flux densities representative of an active galactic nucleus (A) and a starburst nucleus (B), as in Fig. 2. The flux-density ratios for the galaxy IRAS 0857 + 39, for which $R(3.7/1.6) = 26.56$, are indicated in each plot by a short arrow extending from an apparent data point; the vertical position of each arrow gives the appropriate flux-density ratio for this galaxy.

heating radiation in the galaxy increases, as with increased star formation, the equilibrium temperature of the larger dust grains increases, dominating the far-infrared emission and determining the *IRAS* colors.

The data used by Helou (1986) in his analysis were taken from a sample of normal *IRAS* galaxies chosen to exclude likely Seyfert candidates by removing from the sample all galaxies with $R(25/60) > 0.18$; Helou's data are indicated by the dashed envelope in Fig. 6. For comparison, the LBGs with $R(25/60) > 0.18$ have been identified in Fig. 6, although this distinction in $R(25/60)$ does not appear to significantly affect the observed range in $R(12/25)$ or $R(100/60)$ for the LBGs. It is seen that, on average, the LBGs have smaller $R(12/25)$ ratios than do normal *IRAS* galaxies, which, using Helou's model, implies a higher level of star-formation activity in the LBGs. This is consistent with the fact that the LBGs are systematically more luminous than

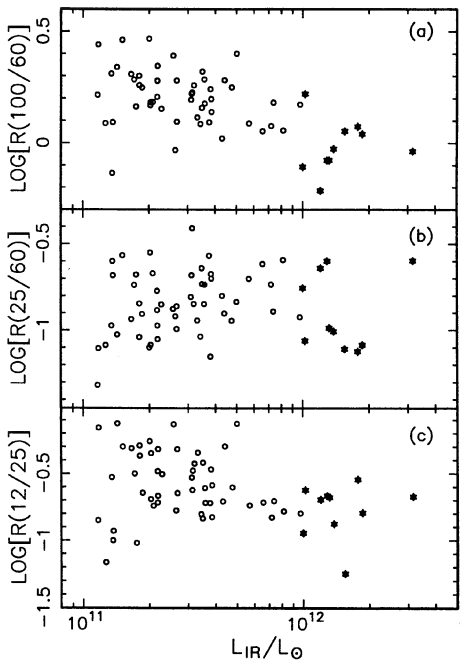

FIG. 4. *IRAS* flux-density ratios $R(100/60)$, $R(25/60)$, and $R(12/25)$ versus the infrared luminosity for the LBGs. The LBGs previously studied by Sanders *et al.* (1988) are plotted with an asterisk.

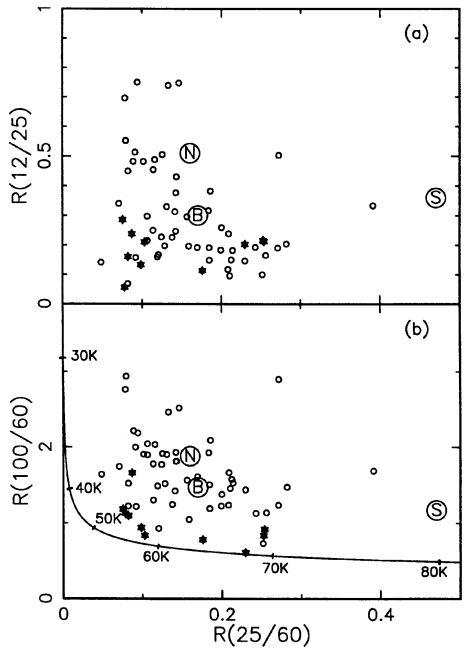

FIG. 5. *IRAS* flux-density ratios, $R(12/25)$, $R(25/60)$, and $R(100/60)$, for the LBGs. The LBGs previously studied by Sanders *et al.* (1988) are plotted with an asterisk. Also shown are the flux-density ratios representative of normal galaxies (N), Seyfert galaxies (S), and starburst galaxies (B), determined using the data of Rowan-Robinson and Crawford (1986). The curve in (b) is the locus of flux-density ratios for dust emission with emissivity proportional to λ^{-1}.

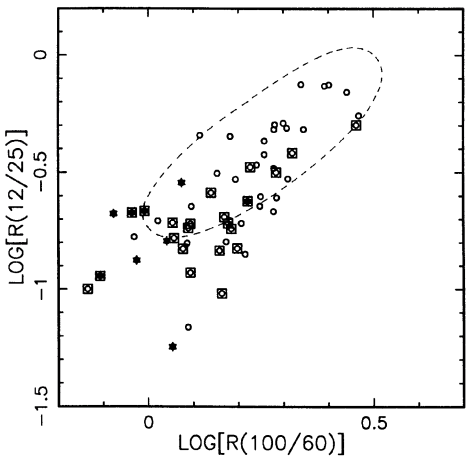

FIG. 6. *IRAS* flux-density ratio $R(12/25)$ versus $R(100/60)$, plotted logarithmically. The LBGs previously studied by Sanders *et al.* (1988) are plotted with an asterisk. The dashed envelope is from a sample of normal *IRAS* galaxies, chosen to exclude likely Seyfert candidates, studied by Helou (1986). Squares indicate LBGs with $R(25/60) > 0.18$ (see the text).

the galaxies in Helou's sample. Furthermore, the luminosity dependence seen in Fig. 4(c) implies that *all* galaxies with $L_{IR} \gtrsim 5\times10^{11}\ L_{\odot}$ have sufficient quantities of large dust grains radiating at high temperatures to dominate the 12 and 25 μm emission. This agrees with the earlier result (Sec. IV*a*) that the infrared luminosity is correlated with hot-dust emission at near-infrared wavelengths.

c) 10 μm Measurements: The Spatial Distribution of the Infrared Emission

The diameter of the 10 μm measuring beam corresponds to a 3 kpc median diameter at the source and a median d_{10}/D_0 of 0.1, where d_{10} is the 10 μm beam diameter and D_0 is the visual major-axis diameter measured from the Palomar Observatory Sky Survey prints. Since the *IRAS* detectors typically subtended 1'.5 × 4'.75, whereas the visual diameter D_0 for the LBGs is typically 0'.2 to 1'.4, the *IRAS* data represent the total emission from each source, independent of D_0. Hence, a comparison of the ground-based 10 μm data, f_ν(10 μm, small beam), with the *IRAS* 12 μm data, f_ν(12 μm, *IRAS*), gives an estimate of the spatial extent of the 10 μm emission in these galaxies. To adjust for the 10–12 μm color, a power law extrapolation through 25 and 12 μm was used to estimate the total 10 μm flux density, f_ν(10 μm, total), for each galaxy, and a second power law extrapolation through 3.7 and 10 μm was used to estimate the 12 μm flux density which would have been measured in a ground-based beam of the same diameter as the 10 μm beam, f_ν(12 μm, small beam). The ratio R_{10} of the 10 μm flux density measured in the ground-based beam to the total 10 μm flux density was then taken as the average of f_ν(10 μm)/f_ν(10 μm, total) and f_ν(12 μm, small beam)/f_ν(12 μm, *IRAS*). Hereafter, R_{10} will be used to characterize the degree of concentration of the 10 μm emission about the nucleus of each galaxy. R_{10} is tabulated in Table IV.

No attempt has been made to correct the values of R_{10} for silicate absorption, which is known to be strong for at least some of these galaxies. In particular, for Arp 220 the visual extinction corresponding to the depth of the silicate feature observed has been estimated by Becklin and Wynn-Williams (1987) to be ~50 mag. In a more detailed analysis than is given here, these authors find that more than 90% of the 12 μm emission from Arp 220 is contained within a 3" diameter about the nucleus, whereas the value of R_{10} presented in this paper for this galaxy is only 0.63. Arp 220 is most likely a very extreme case, but nevertheless, more accurate values for R_{10} would be somewhat higher than those presented here.

The extent of the 10 μm emission is potentially an effective diagnostic of the relative AGN contribution in a galaxy, since dust sufficiently hot to radiate in a steady state at 10 μm must be at a temperature of several hundred degrees, and hence must be comparatively close to the luminosity source. For dust at 300 K (which corresponds to a peak in the thermal energy distribution at 10 μm, if the dust emissivity is proportional to frequency), illuminated by a source of luminosity $\sim 5\times10^{11}\ L_{\odot}$, characteristic distances are on the order of one hundred to a few hundred parsecs. Thus, substantial 10 μm emission beyond this distance from the nucleus cannot be due to dust directly heated by an AGN, and should generally be attributed to a distributed luminosity source, such as star formation.

In Fig. 7, the fraction of the total 10 μm emission within the ground-based 10 μm beam is shown for the LBGs, by plotting R_{10} versus the 10 μm beam diameter, in kiloparsecs at the source. Most of the galaxies have significant 10 μm emission beyond 1 kpc in diameter, providing evidence that enhanced star formation contributes substantially to the intrinsic luminosity in most of the LBGs. The possible exceptions to this are those galaxies with $R_{10} \sim 1$, for which the 10 μm diameter is an upper limit on the spatial extent of the 10 μm emission.

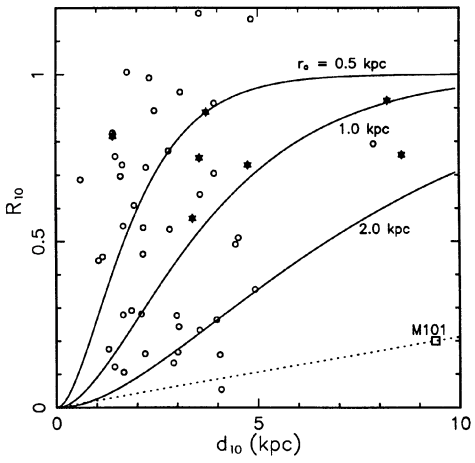

FIG. 7. Fraction of the total 10 μm emission measured in a 5" beam plotted as a function of the 10 μm beam diameter, in kiloparsecs source. Galaxies with only limits at 10 μm or 12 μm (see Table II) have not been included. The LBGs previously studied by Sanders *et al.* (1988) are plotted with an asterisk. The curves indicate exponential brightness distributions where the surface brightness falls to 1% of its peak brightness at a radius $D/2$ (see the text); curves have been drawn for $r_0 = 0.5$, 1.0, and 2.0. The 10 μm emission within a 9.4 kpc diameter about the nucleus of M101 is shown for comparison (Rice 1987).

An estimate of the extent of the 10 μm emission in the galaxy M101 has been indicated in Fig. 7 by plotting the 12 μm emission within a 9.4 kpc diameter about its nucleus (Rice 1987). It is clear that the 10 μm emission in M101 is more extended than that in most of the LBGs. M101 was chosen for comparison to the LBGs because it is representative of gas-rich spiral galaxies of moderate luminosity detected by *IRAS* (from Paper I, the luminosity of M101 is 2×10^{10} $L_\odot$), and is large enough for information on the spatial distribution to be obtained. The *IRAS* data for two other moderate-luminosity gas-rich spirals, M51 and NGC 891, yield results very similar to that of M101 (Rice).

Also shown in Fig. 7 are flux integrals for a brightness distribution proportional to $\exp(-r/r_0)$, with $r_0 = 0.5$, 1.0, and 2.0 kpc. An exponential brightness distribution corresponds to the disk emission in normal spiral galaxies (see, for example, Mihalas and Binney 1968). Most of the LBGs have irregular morphologies, in many cases apparently due to galaxy collisions, so it is unlikely that their brightness profiles would be well represented by an exponential law. Nevertheless, the exponential scale size r_0 can be a useful number for characterizing the breadth of the light distribution. It is seen that roughly one-third of the LBGs have scale sizes $r_0 \leqslant 0.5$ kpc, a size Hill (1987) has shown to be characteristic of a compact nuclear infrared source.

Although 10 μm emission beyond 1 kpc of the center of a galaxy must be due to a distributed source, such emission does not preclude the possibility of an additional, substantial contribution to the total luminosity from a central point source. By assuming that the 10 μm emission coming from *outside* of the ground-based beam has a brightness profile appropriate for normal-galaxy disk emission, and by setting a limit to the diameter out to which this 10 μm disk emission originates, one can estimate the maximum possible contribution to the 10 μm emission from a central point source which is consistent with the observed value for R_{10}. Since no galaxies are yet known where significant 12 μm emission is detected beyond the optical disk (Rice *et al.* 1987) D_0 can be taken as a limit to the extent of the 10 μm disk emission. An estimate, R_{PS} of the maximum possible point-source contribution to the observed 10 μm flux density for each of the LBGs was thus obtained by modeling the spatial distribution of the 10 μm emission as a central point source coupled with an exponential disk whose surface brightness drops to 1% of its peak brightness at a radius $D_0/2$. The results are shown in Fig. 8, for the entire LBG sample and also for the LBGs with $L_{IR} \geqslant 10^{12}$ $L_\odot$. The data for roughly two-thirds of the LBGs are consistent with a contribution of 20% or more to the total 10 μm emission from a central point source, and half of the galaxies are consistent with a contribution of 50% or more from a point source.

Figure 8 also shows a possible luminosity dependence for the degree of concentration of the 10 μm emission, since six of the seven galaxies with $L_{IR} \geqslant 10^{12}$ $L_\odot$ plotted in the histogram have $R_{PS} \geqslant 0.4$. This possible luminosity dependence has been investigated further in Fig. 9, which shows R_{10} plotted against the infrared luminosity for the LBGs. There does not appear to be any luminosity dependence in R_{10}, for luminosities below approximately 7×10^{11} $L_\odot$. However, the population of galaxies with broadly extended 10 μm emission does decrease abruptly above this luminosity. This is not a selection effect since, for galaxies with angular diameter less than 50″ (a size that includes 12 of the 14 LBGs with $L_{IR} > 7\times10^{11}$ $L_\odot$), there is no correlation between R_{10} and optical diameter.

V. CONCLUSIONS

An analysis of 61 *IRAS* galaxies with infrared luminosities greater than or equal to 10^{11} $L_\odot$ has yielded the following results:

(1) An increase in the total infrared luminosity above $L_{IR} \sim 10^{11}$ $L_\odot$ is correlated with increased emission from hot dust with characteristic temperatures $\sim$800 K. This hot dust contributes a substantial fraction of the 2.2 and 3.7 μm emission, resulting in a greatly increased dispersion in $R(3.7/1.6)$ and $R(2.2/1.6)$ for such galaxies relative to lower-luminosity galaxies. This excess hot-dust emission ap-

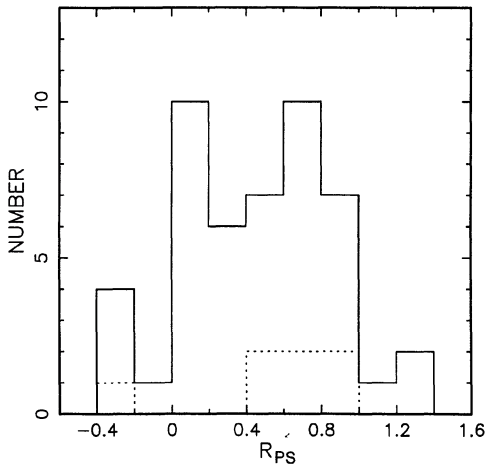

FIG. 8. Histograms of the maximum possible contribution to the 10 μm emission from a central point source, R_{PS} (see the text). Solid line: the LBG sample; dotted line: the LBGs with $L_{IR} \geqslant 10^{12}$ $L_\odot$. Galaxies with only limits at 10 or 12 μm (see Table II) have not been included in either histogram.

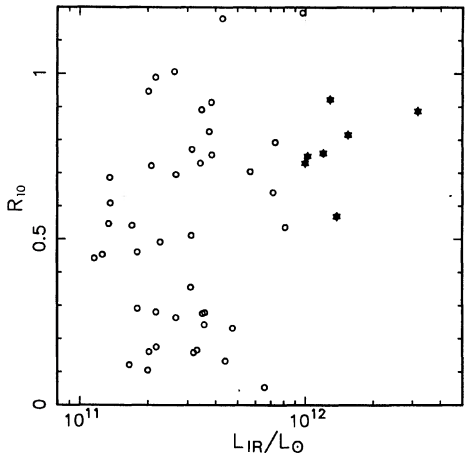

FIG. 9. The ratio R_{10} of the 10 μm emission in the ground-based beam to the total 10 μm emission, versus the infrared luminosity for the LBGs. Galaxies with only limits at 10 or 12 μm (see Table II) have not been included. The LBGs previously studied by Sanders *et al.* (1988) are plotted with an asterisk.

pears to "turn on" at luminosities $\sim 10^{11} L_{\odot}$. Galaxies with the largest contribution to the near-infrared emission from hot dust have systematically smaller $R(10/3.7)$ ratios, which may represent a shift in the temperature of the dust to hotter temperatures in these galaxies, but can also be explained as an increase in silicate absorption due to an increase in the mass of dust in these galaxies.

(2) The far-infrared flux-density ratios of very luminous infrared galaxies generally span the range from normal to "starburst" galaxies, but a number of the galaxies studied have steeper energy distributions between 12 and 25 μm than are expected from normal or starburst galaxies. None of the galaxies presented in this paper have flux-density ratios appropriate for typical Seyfert galaxies.

(3) The far-infrared emission in very luminous infrared galaxies cannot be modeled with a single dust temperature, but requires a contribution from cold dust ($T \sim 30$–50 K) coupled with a warmer component with characteristic temperatures $T \gtrsim 70$ K. Although the maximum cold-dust contribution seen in infrared galaxies decreases at luminosities above $10^{11} L_{\odot}$, the temperature of the warmer component does not change with luminosity.

(4) If one adopts the model of Helou (1986), the $R(12/25)$ and $R(100/60)$ ratios in the LBGs indicate systematically higher levels of star-formation activity in extremely luminous infrared galaxies as compared to normal *IRAS* galaxies. For galaxies with $L_{IR} \gtrsim 5 \times 10^{11} L_{\odot}$, the $R(12/25)$ ratio is dominated by emission from large dust grains radiating at high temperatures rather than from PAHs.

(5) Most of the LBGs emit a significant fraction of their 10 μm emission beyond 1 kpc, indicating a substantial contribution to their luminosities from star formation. However, one-third of the galaxies have exponential scale sizes characteristic of compact sources, and half of the galaxies have 10 μm emission consistent with a contribution of 50% or more from a central point source.

(6) There is no correlation between the degree of concentration of the 10 μm emission and luminosity for luminosities less than about $7 \times 10^{11} L_{\odot}$. However, above this luminosity the population of galaxies with extended 10 μm emission decreases abruptly.

The authors thank Walter Rice for the data on M101, and the night assistants at the Palomar 200 in. telescope, Juan Carrasco and Skip Staples. Thanks is also given to the entire staff at IPAC and Palomar Observatory. This work was supported by a grant from the National Science Foundation, and by NASA through the *IRAS* Extended Mission program.

REFERENCES

Aaronson, M. (1977). Ph.D. thesis, Harvard University.
Becklin, E. E., and Wynn-Williams, C. G. (1987). In *Star Formation in Galaxies*, edited by C. J. Lonsdale Persson, NASA Conf. Publ. No. 2466 (NASA, Washington, DC), p. 643.
Becklin, E. E., Fomalont, E. B., and Neugebauer, G. (1973). Astrophys. J. Lett. **181**, L27.
Beichman, C. A., Neugebauer, G., Habing, H. J., Clegg, P. E., and Chester, T. J., editors (1985). *IRAS Explanatory Supplement* (U.S. GPO, Washington, DC).
Carico, D. P., Soifer, B. T., Beichman, C,. Elias, J. H., Matthews, K., and Neugebauer, G. (1986). Astron. J. **92**, 1254.
Cohen, J. G., Frogel, J. A., Persson, S. E., and Elias, J. H. (1981). Astrophys. J. **249**, 481.
de Jong, T., Clegg, P. E., Soifer, B. T., Rowan-Robinson, M., Habing, H. J., Houck, J. R., Aumann, H. H., and Raimon, E. (1984). Astrophys. J. Lett. **278**, L67.
Désert, F. X. (1986). In *Light On Dark Matter*, edited by F. P. Israel (Reidel, Dordrecht), p. 213.
Draine, B. T., and Lee, H. M. (1984). Astrophys. J. **285**, 89.
Eales, S. A., Wynn-Williams, C. G., and Beichman, C. A. (1988). In preparation.
Elias, J. H., Frogel, J. A., Matthews, K., and Neugebauer, G. (1982). Astron. J. **87**, 1029.
Elston, R., Cornell, M. E., and Lebofsky, M. J. (1985). Astrophys. J. **296**, 106.
Helou, G. (1986). Astrophys. J. Lett. **311**, L33.
Hill, G. J. (1987). In *Star Formation in Galaxies*, edited by C. J. Lonsdale Persson, NASA Conf. Publ. No. 2466 (NASA, Washington, DC), p. 611.
IRAS Point Source Catalog (1985). (U.S. GPO, Washington, DC).
Lawrence, A., Ward, M., Elvis, M., Fabbiano, G., Willner, S. P., Carleton, N. P., and Longmore, A. (1985). Astrophys. J. **291**, 117.
Léger, A., and Puget, J. L. (1984). Astron. Astrophys. **137**, L5.
Lonsdale, C. J., Helou, J. C., Good, J. C., and Rice, W., compilers (1985). *Cataloged Galaxies and Quasars Observed in the IRAS Survey*, JPL Publ. No. D1932 (internal document).
Mihalas, D., and Binney, J. (1986). *Galactic Astronomy* (Freeman, San Francisco), p. 323.
Miley, G. K., Neugebauer, G., and Soifer, B. T. (1985). Astrophys. J. Lett. **293**, L11.
Neugebauer, G., Green, R. F., Matthews, K., Schmidt, M., Soifer, B. T., and Bennett, J. (1987). Astrophys. J. Suppl. **63**, 615.
Pérault, M., Boulanger, F., Puget, J. L., and Falgarone, E. (1987). Astron. Astrophys. (submitted).
Puget, J. L., Léger, A., and Boulanger, F. (1985). Astron. Astrophys. **142**, L19.
Rice, W. (1987). Private communication.
Rice, W., Lonsdale, C. J., Soifer, B. T., Neugebauer, G., Kopan, E. L., Lloyd, L. A., De Jong, T., and Habing, H. J. (1987). *A Catalog of IRAS Observations of Large Optical Galaxies* (Jet Propulsion Laboratory, Pasadena) (in press).
Rieke, G. H., Lebofsky, M. J., Thompson, R. I., Low, F. J., and Tokunaga, A. T. (1980). Astrophys. J. **238**, 24.
Rowan-Robinson, M., and Crawford, J. (1986). In *Light On Dark Matter*, edited by F. P. Israel (Reidel, Dordrecht), p. 421.
Sanders, D. B., Soifer, B. T., Elias, J. H. Madore, B. F., Matthews, K., Neugebauer, G., and Scoville, N. Z. (1988). Astrophys. J. **325**, 74.
Scoville, N. Z., Soifer, B. T., Neugebauer, G., Young, J. S., Matthews, K., and Yerka, J. (1985). Astrophys. J. **289**, 129.
Sekiguchi, K. (1987). Astrophys. J. **316**, 145.
Sellgren, K. (1984). Astrophys. J. **277**, 623.
Smith, B. J., Kleinmann, S. G., Huchra, J. P., and Low, F. J. (1987). Astrophys. J. **318**, 161.
Soifer, B. T., Sanders, D. B., Madore, B., Neugebauer, G., Danielson, G. E., Elias, J. H., Persson, C. J., and Rice, W. L. (1987). Astrophys. J. **320**, 238 (Paper I).
Soifer, B. T., *et al.* (1984). Astrophys. J. Lett. **278**, L71.
Tokunaga, A. (1984). Astron. J. **89**, 172.